

# Leading-colour-based unweighted event generation for multi-parton tree-level processes

Rikkert Frederix<sup>1,\*</sup>, Timea Vitos<sup>2,3†</sup>

<sup>1</sup> *Department of Physics, Lund University,  
Sölvegatan 14A, SE-223 62, Lund, Sweden*

<sup>2</sup> *Department of Physics and Astronomy, Uppsala University,  
Box 516, 751 20, Uppsala, Sweden*

<sup>3</sup> *Institute for Theoretical Physics, ELTE Eötvös Loránd University  
Pázmány Péter sétány 1/A, H-1117 Budapest, Hungary*

## Abstract

In this work, we revisit unweighted event generation for multi-parton tree-level processes in massless QCD. We introduce a two-step approach, in which initially unweighted events are generated at leading-colour (LC) accuracy, followed by a reweighting of these events to full-colour (FC) accuracy and applying an additional unweighting cycle. This method leverages the simple structure of LC integrands, enabling optimized phase-space parameterisations and resulting in high primary unweighting efficiencies, ranging from the percent level for  $2 \rightarrow 4$  processes to the per-mille level for  $2 \rightarrow 7$  processes. Given that the LC-accurate matrix elements closely approximate the FC-accurate ones, the secondary unweighting efficiencies exceed 50%. Our results suggest that this two-step approach offers an efficient alternative to direct event generation at FC accuracy.

---

\*E-mail: rikkert.frederix@fysik.lu.se

†E-mail: timea.vitos@physics.uu.se

# Contents

<b>1</b>	<b>Introduction</b>	<b>2</b>
<b>2</b>	<b>Two-step event generation</b>	<b>3</b>
2.1	The approximation of the matrix elements . . . . .	4
2.1.1	Leading-colour matrix elements . . . . .	4
2.1.2	Phase-space generation . . . . .	5
2.2	Reweighting and secondary unweighting . . . . .	8
<b>3</b>	<b>Results</b>	<b>9</b>
3.1	Setup . . . . .	9
3.2	Numerical results for fixed partonic collision energy . . . . .	11
3.3	Numerical results for the LHC setup . . . . .	14
<b>4</b>	<b>Conclusions and Outlook</b>	<b>23</b>

## 1 Introduction

In preparation for the large amount of data to be collected during the upcoming high-luminosity phase of the Large Hadron Collider (LHC), improvements and developments in accuracy and precision of the theoretical description of both background and signal processes are essential. Because of the nature of hadronic collisions and the intrinsic properties of quantum chromodynamics (QCD), interesting (signal) events are often accompanied by multiple well-separated hadronic jets—either as part of the signal, or as a background to it. Predictions for cross sections and differential distributions for such processes are time-consuming to compute, even at leading order (LO) in perturbation theory, since they entail high-dimensional ( $3n - 2$ , with  $n$  the number of final-state particles) phase-space integrals of integrands whose complexity increases factorially with  $n$ . Ideally, these predictions come in the form of *unweighted events*, meaning events distributed according to a probability density function proportional to the magnitude of the integrand. In practice, the only viable options to perform these integrals are numerical (Monte Carlo) methods, combined with a hit-or-miss step to obtain unweighted events.

In order to improve the efficiency of the integration, techniques such as importance sampling [1–3], and multi-channeling [4, 5] are employed [6–12]. Moreover, determining the optimal parametrisation of the phase space with respect to the integration variables is crucial for efficient integration. Generating the momenta uniformly [13, 14] is typically not desirable; parametrisations in which integration variables are linked to invariants that enter the propagator structure of the Feynman diagrams contributing to the process under consideration [15, 16] yield greater integration efficiency. Alternatively to using the propagator structure, approaches presented in Refs. [17, 18] use the antenna structure of the QCD matrix elements as part of the phase-space parametrisation. More recently, parametrisations that align the most-common variables on which physical phase-space cuts are applied with integration variables have been proposed [19]. Going beyond the analytic transformations to flatten the integrand, multivariate machine learning algorithms are also under development to improve the efficiency in phase-space integration [20–31].

In addition to improving the integration, to address the factorial growth in complexity of the integrand, techniques involving recursion relations and/or Monte Carlo sampling of helicities and colours of the external particles have been employed [10, 32–38].

In this work, we revisit the method of unweighted event generation for multi-parton tree-level processes in QCD. We propose an approach in which an approximation of the complete LO-accurate matrix elements is used in a first, integration, step. Unweighted events are generated in this approximation. As a second step, these generated events are reweighted to the exact LO-accurate matrix elements, and a secondary unweighting step is performed.

Our paper is structured as follows. In Sec. 2 we discuss the details of our method, i.e., the approximation used for the integrand, as well as the four different phase-space parametrisations that we have considered for the integration step of our method. In Sec. 3 we present our findings for the primary and secondary unweighting efficiencies in an idealised, fixed-energy partonic collision as well as in a more realistic LHC setup, taking parton distribution functions into account. In the final section we conclude and give a short outlook on the results presented.

## 2 Two-step event generation

Multi-parton matrix elements are slow to evaluate, they have non-trivial structures, and the corresponding phase space has a high dimensionality, resulting in a large variance in the weights of the generated phase-space points. For the generation of unweighted events, i.e., events that are distributed according to the density of the integrand (and hence all assigned the same weight, or, contribution, to the integrand evaluation), the weight of each event needs to be compared to the maximum possible weight and is kept with a probability equal to the ratio of its weight to the maximum weight. The fraction of events kept in this way is what is commonly referred to as the unweighting efficiency. Since there can easily be multiple orders of magnitude between typical event weights and the maximum weight, the unweighting efficiencies for multi-parton processes can be quite low, which is problematic when the evaluation time of the matrix elements is long.

The idea behind our method is to split this event generation procedure into two (or more) steps. In the first step, an approximation of the integrand is used that reduces it to a simple form, making it very fast to evaluate, and unweighted events are generated from this integrand. Besides the requirement that the evaluation time of the approximated integrand must be short, using a simple integrand has the additional benefit that it is easier to find a good phase-space parametrisation that reduces the variance in the generated weights, resulting in an improved unweighting efficiency. In the subsequent step(s), these low-accuracy events are reweighted to higher accuracy<sup>1</sup>. For these reweight factors, the full (tree-level) time-consuming matrix elements need to be evaluated. However, only for the smaller set of phase-space points corresponding to the unweighted events generated in the first step. The resulting weighted events can be unweighted again by keeping them with a probability equal to the ratio of their reweight factors to the maximum possible reweight factor, ensuring that the final set of events with unit weights follows the exact distribution of the initial integrand.

For this method to work efficiently, the approximation must fulfill some basic properties. Firstly, it needs to be fast to evaluate, and/or an efficient parametrisation of the phase space must exist such that peaks in the integrand can be flattened accordingly. Furthermore, the reweight factors which are needed to go from the approximation to the full-accuracy events must have a small variance, i.e., the approximation cannot be too inaccurate and must closely follow the full integrand in all of phase space. If the variance is too large, the secondary unweighting of the full-accuracy events can be rather inefficient, resulting in a poor overall performance. It would be particularly problematic if the

---

<sup>1</sup>Our work is focused on tree-level accuracy within perturbative QCD, and thus a full accuracy is never obtained. Here, high- and full-accuracy refer to the level of approximation of the integrand, which is, by itself, a tree-level approximation of the scattering process.

approximation grossly underestimated the full-accurate matrix elements in a particular phase-space region, resulting in extremely large reweight factors, which would completely spoil the efficiency of the secondary unweighting. However, the approximation does not have to get the overall normalisation of the full-accuracy result right: a constant offset does not affect the secondary unweighting efficiency.

The general process we consider is the scattering of two incoming partons into  $n$  final-state partons which are labeled according to

$$ab \rightarrow 12 \dots n. \quad (1)$$

The integral which is to be computed for this process is the integral in the phase space over the squared matrix elements, averaged over initial colour and helicity and summed over all external assignments, convoluted with the two parton distribution functions (for a hadronic collision setup), and including the flux factor, schematically,

$$\sigma_{ab \rightarrow 12 \dots n} = \int |\mathcal{M}|^2 d\Phi, \quad (2)$$

where we have suppressed the flux factor and the parton luminosity factors. The phase-space measure includes the Bjorken- $x$  variables,  $d\Phi = dx_a dx_b d\Phi_n$ , with  $d\Phi_n$  denoting the usual Lorentz-invariant phase-space measure for  $n$  final-state partons.

## 2.1 The approximation of the matrix elements

As the approximation of the integrand under consideration, we use the leading-colour (LC) approximation of the matrix elements, obtained by performing a large- $N_c$  ( $N_c$  being the number of colours) expansion. Since the structure of the matrix elements at this accuracy is rather simple, efficient phase-space generators can be developed in this approximation. As shown later, the LC matrix elements form an excellent approximation of the integral at full-colour (FC) accuracy, and result in a narrow weight distribution for the reweight factors.

### 2.1.1 Leading-colour matrix elements

The amplitudes appearing in the integrand are summed over colour and helicity configurations of the external particles. They can be decomposed into colour-ordered amplitudes, which are dependent on the colour ordering of the external particles. In general, the colour ordering can be expressed as an ordered string of the particle labels, such as  $(a123b45)$  for  $n = 5$  final-state particles. In this ordering, if quarks are present in the process, a quark label always appears first in the order and an anti-quark label always last. Depending on the particle content, this sequence can be cyclically invariant (all-gluon processes), fixed (for one-quark line processes), or redundant in the exchange of a substring that begins with a quark label and ends with an anti-quark label (for processes with multiple quark lines). At leading colour, all interferences between different colour-ordered amplitudes vanish. Schematically, using, e.g. the decomposition of the matrix elements based on the fundamental basis<sup>2</sup>,

$$\int |\mathcal{M}|^2 d\Phi = \int \sum_{i,j} \mathcal{A}_i C_{ij} \mathcal{A}_j^* d\Phi \xrightarrow{\text{LC}} \int \sum_i \mathcal{A}_i C_{ii} \mathcal{A}_i^* d\Phi = \sum_i C_{ii} \int |\mathcal{A}_i|^2 d\Phi, \quad (3)$$

---

<sup>2</sup>There are other bases, such as the multiplet basis [39], that are also diagonal at full colour. However, for those cases, the basis elements are no longer single colour-ordered amplitudes, and therefore much slower to evaluate.

where, in the final step, we have taken the sum outside of the integral sign, which emphasizes that each term in the sum can be integrated separately. Note that for processes with (at least) two different-flavour quark lines, all the elements on the diagonal of the colour matrix are considered in our LC approximation as the notation in Eq. (3) suggests, even though only half of them contribute at LC and the other half starts only at next-to-leading-colour (NLC) accuracy in the colour expansion, see e.g. Ref. [40]. In general, the number of elements in the sum grows factorially with the number of external particles. However, many elements in the sum yield the same result since the phase space is symmetric for identical particles, and, in practice, the number of separate integrals one needs to consider scales, at worst, polynomially with the number of external particles [40, 41]. Moreover, using recursion relations, such as the ones introduced in e.g. Refs. [32, 42], a single colour ordering for a given helicity configuration can be computed with, at most, exponential scaling with the number of external particles.

For the parton multiplicities we consider (up to  $n \simeq 7$ ), it is more efficient to explicitly sum over all helicities of the colour-ordered amplitudes for each phase-space point, instead of sampling over them. The reason is that sampling over helicities increases the variance of the matrix elements in the phase-space integration, leading to a poorer performance and decreased unweighting efficiencies<sup>3</sup>. Before writing the unweighted LC-accurate events to the event file, we assign them one helicity configuration randomly, weighted by their relative contributions. The subsequent reweighting steps are therefore performed for a single helicity configuration.

### 2.1.2 Phase-space generation

The general  $n$ -body phase-space measure, including the two initial-state Bjorken- $x$  momentum fraction factors relevant for hadron-hadron collisions, is proportional to

$$dx_a dx_b d\Phi_n = dx_a dx_b \left( \prod_{i=1}^n d^4 p_i \delta(p_i^2 - m_i^2) \Theta(E_i) \right) \delta^{(4)} \left( p_a + p_b - \sum_{i=1}^n p_i \right), \quad (4)$$

where  $p_a$  and  $p_b$  are the four-momenta of the right- and left-incoming particles, and  $p_i$  and  $m_i$  are the four-momenta and masses of the  $n$  final-state particles. For simplicity, in the expression we have suppressed factors of  $2\pi$ . For an implementation in a numerical code, the delta-functions need to be resolved. Typically, but not necessarily, this is done by combining each of the  $\delta(p_i^2 - m_i^2)$  factors with the corresponding  $d^4 p_i$  measures into  $d^4 p_i \delta(p_i^2 - m_i^2) = \frac{d^3 \mathbf{p}_i}{2E_i}$ , and the four-dimensional delta-function imposing overall momentum conservation,  $\delta^{(4)} \left( p_a + p_b - \sum_{i=1}^n p_i \right)$ , is used to express the momentum of, without loss of generality, particle  $n$  in terms of the momenta of the other particles (as well as one of the integration variables relevant for particle  $n - 1$ ). Most-conveniently, this allows for a sequential generation of the phase space, whereby, typically, first the momenta of the two incoming particles are generated by throwing random numbers for  $x_a$  and  $x_b$ , and then using  $(n - 2)$  universal blocks, each consisting of three random variables to generate the momenta of particles  $1 \dots n - 2$  by splitting, for each particle  $i$ , the remaining momentum  $p_{r+i} \rightarrow p_r + p_i$ , as depicted in Fig. 1. The last particle  $n - 1$  can be generated using a slightly modified building block, containing only 2 random variables, while the momentum of particle  $n$  follows directly from momentum conservation once all the momenta of particles  $1 \dots n - 1$  are known.

In the universal blocks the three random variables can, in principle, directly correspond to the Cartesian  $x$ ,  $y$ , and  $z$  components of the momentum  $p_i$ , but it is more efficient to perform

---

<sup>3</sup>This has been directly checked and verified.

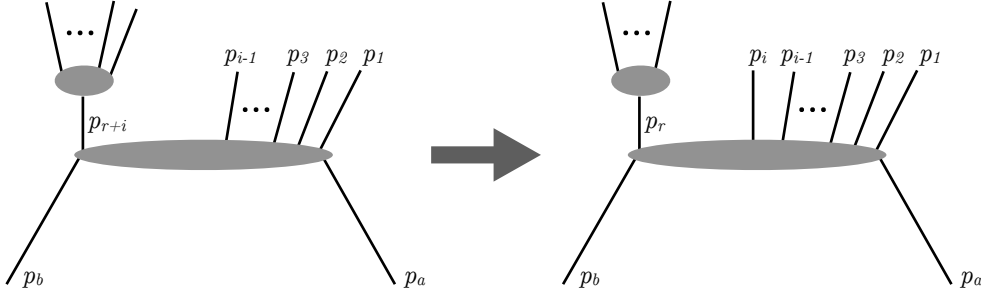


Figure 1: The step to generate the momentum of particle  $i$  in the sequential phase-space generation: a pseudo-particle with momentum  $p_{r+i}$  is split into a (pseudo-)particle with momentum  $p_r$  and a particle with momentum  $p_i$ .

a change of variables and relate these to variables that are directly relevant in matrix elements. In particular one would like the peaks in the integrand of the phase-space integral to align with the integration variables, such that a (non-uniform) generation of the random variables (either through one-dimensional analytic transformations or numerical methods such as the Vegas algorithm [1, 2]) can flatten the peaks, which reduces the variance among the weights of the generated phase-space points and improves unweighting efficiency.

For the processes that we consider in this work, the strongest peaks follow the antenna structure of the colour-ordered QCD amplitudes<sup>4</sup>. This is particularly evident in the maximally helicity violating (MHV) amplitudes for the all-gluon process, that take a particularly simple form [43], e.g.,

$$|\mathcal{A}_i|^2 \propto \frac{(p_a \cdot p_b)^4}{(p_a \cdot p_b)(p_b \cdot p_1)(p_1 \cdot p_2) \cdots (p_n \cdot p_a)}, \quad (5)$$

corresponding to particles  $a$  and  $b$  having opposite helicity to particles  $1, \dots, n$  and corresponding to the colour ordering  $(ab1 \dots n)$ . For non-MHV helicity configurations, the amplitudes take on slightly more complicated forms, see, e.g. Ref. [44], but the overall structure remains. Therefore, the natural ordering in which to generate the phase-space splittings, c.f. Fig. 1, is according to the colour ordering<sup>5</sup>. If the two incoming particles are adjacent in the colour ordering under consideration, we generate the phase space in the same sequence as the colour ordering. If, on the other hand, the two incoming particles are not adjacent, we first perform an overall  $p_a + p_b \rightarrow p_{r_1} + p_{r_2}$  phase-space generation, in which  $p_{r_1}$  corresponds to the combined momenta of the particles in the colour ordering between particles  $a$  and  $b$ , and  $p_{r_2}$  to the combined momenta between particles  $b$  and  $a$ . For each of these sets, we then perform the splittings  $p_{r_{1,2}} \rightarrow p_{r_{1,2}-i} + p_i$  sequentially, following the colour ordering as depicted in Fig. 1.

We consider the following four phase-space parametrisations, each of which uses different integration variables in the universal blocks.

1. The **Haag** phase-space generation method [18] has been designed to generate the phase-space density directly according to the all-gluon MHV matrix elements, Eq. (5). In the universal

<sup>4</sup>While the actual divergence needs to be removed by phase-space cuts, dominant contributions to the integral still come from the phase-space regions close to these cuts.

<sup>5</sup>Also for processes with quarks, we take the (or, if there are several, one of the) naive colour ordering(s) (and assume invariance under cyclic permutations) as the sequence in the phase-space generation. This is reasonable since colour-ordered amplitude with quarks have fewer peaks than all-gluon amplitudes.

blocks used for the momentum split  $p_{r+i} \rightarrow p_r + p_i$ , this parametrisation uses rescaled invariants between the momenta  $p_i$  and  $p_{i-1}$  and the momenta  $p_r$  and  $p_a$  (or  $p_b$ ), as well as the invariant mass of  $p_r$ , as the three integration variables (with the latter omitted to generate the momentum of particle  $n - 1$ ). In order to get the correct overall density, the generation of these variables must be performed following specific densities [18].

2. The **t-channel** method [16] uses building blocks for the  $p_{r+i} \rightarrow p_r + p_i$  momentum split in which the invariant computed from the momenta  $p_r$  and  $p_a$  (or  $p_b$ ), i.e., the “ $t$ -channel” momentum, and the invariant mass of  $p_r$  are used as integration variables. The third variable is the azimuthal angle of  $p_i$ , defined in the frame where the momentum  $p_{r+i}$  is at rest. Since, in the high-energy limit, the matrix elements are dominated by  $t$ -channel structures, see also e.g. Ref. [45], it is expected that this parametrisation works well for multi-particle processes.
3. An extension to the  $t$ -channel method, to increase the number of invariants used as integration variables, was first described in Ref. [15]. This method is similar to the  $t$ -channel method in that it uses the invariant mass of the remaining momentum and the invariant computed from the current momentum with one of the initial-state momenta as integration variables. On the other hand, the azimuthal angle is replaced by the invariant mass between the current and the previously generated momentum  $(p_i + p_{i-1})^2$ . Since it requires there to be two final-state (pseudo-)particles, the ones with momentum  $p_{r+i}$  and  $p_{i-1}$  (see Fig. 1), to generate the third momentum  $p_i$ , we have dubbed this method **gen2→3**. It uses very similar variables as the Haag method, such that all the invariants appearing in the MHV antenna structure, Eq. (5), can be mapped directly to integration variables<sup>6</sup>. However, it is not enforced that the density of the generated momenta exactly corresponds to the MHV antenna structure, rather, it relies on (numerical) importance sampling, as implemented in the Vegas algorithm, to generate momenta as close as possible to the density of the integrand. This has the advantage that the algorithm is much simpler than the Haag one. Even though this method was developed in the late 1960s, this is, to the best of our knowledge, the first time that this phase-space parametrisation has been implemented and used to generate the phase space for general multi-particle processes.
4. The  **$p_T$ -based** method introduced in Ref. [19], uses the transverse-momentum, the rapidity and the azimuthal angle of particle  $i$  as integration variables in the universal blocks (all in the laboratory frame). Since each of the blocks are independent, it can be seen as a baseline method that does not incorporate any of the structure of the colour-ordered antennae in the phase-space generator. On the other hand, it has the advantage that the LHC analyses typically impose analysis cuts on transverse momenta and rapidities of final-state objects, which are aligned with the integration variables in this method. Therefore, importance-sampling grids can also optimise precisely close to these phase-space boundaries. Moreover, contrary to the previous three methods, this method does not start with generating the momenta of the two incoming particles. Rather, the integration variables relevant to the two Bjorken  $x$ ’s are transformed such that  $n - 1$  universal blocks are used (instead of  $n - 2$ ), and the final variable is transformed to the overall rapidity of the system, which then defines the momenta of the two incoming particles in terms of the final-state ones and this variable. See Ref. [19] for details.

---

<sup>6</sup>With a couple of exceptions: for  $2 \rightarrow 2$  scattering at fixed partonic energy, there are only two independent integration variables, while the denominator in Eq. (5) contains four invariants (which are obviously not independent). For higher multiplicities, we generate the phase space separately for the final-state particles between the two incoming particles  $a$  and  $b$  and particles  $b$  and  $a$  in the colour ordering. If one of these two sets contains exactly one or two particles, the invariants related to that set are not all directly mapped to integration variables.

Since the first three methods have the two Bjorken  $x$ 's as integration variables, they can also be used for fixed-energy lepton collisions, by simply setting  $x_a = x_b = 1$  instead of generating them. The  $p_T$ -based integration is thus only evaluated in the “LHC setup”, described in the Results section.

## 2.2 Reweighting and secondary unweighting

Once the unweighted events following the density of the LC-accurate matrix elements have been generated using the integration techniques described above, they can be reweighted to improve their accuracy. We consider the reweighting of events both to next-to-leading colour (NLC) and full-colour accuracy, using the reweight factors

$$r^{\text{LC} \rightarrow \text{NLC}} = \frac{|\mathcal{M}^{\text{NLC}}|^2}{\sum_i C_{ii} |\mathcal{A}_i|^2}, \quad \text{and} \quad r^{\text{LC} \rightarrow \text{FC}} = \frac{|\mathcal{M}|^2}{\sum_i C_{ii} |\mathcal{A}_i|^2}, \quad (6)$$

in which  $|\mathcal{M}^{\text{NLC}}|^2$  and  $|\mathcal{M}|^2$  are the matrix elements summed over the colours of the external particles, up to next-to-leading- and full-colour accuracy, respectively. These factors are phase-space-point dependent and need to be computed for each LC event separately. Since the external particles in LC events have assigned helicities, only the helicity configuration chosen for each event needs to be considered in both the numerator and denominator of the reweight factors, with no helicity sum required.

Note that the LC events have been generated only in a subset of all the available channels, i.e., only a subset of the elements in the sum on the r.h.s. of Eq.(3) need to be taken into account, since the other contributions can be obtained by swapping identical final-state particles. However, in the denominators in Eq. (6) all the elements in the sum need to be taken into account in the colour ordering to get the correct distribution of NLC or FC accuracy events.<sup>7</sup>

The secondary unweighting is performed in the usual manner, in which a weighted event  $i$  is accepted if its reweight factor satisfies

$$\frac{r_i}{r_{\max}} > R, \quad (7)$$

where  $R$  is a uniformly distributed random number between 0 and 1, and  $r_{\max}$  is the maximum possible reweight factor. In practice, the maximum possible reweight factor is unknown, but a good proxy is the maximum reweight factor found among all the events that are considered in the reweighting<sup>8</sup>.

Note that, depending on the accuracy of the LC and NLC approximations and the relative timing of evaluating the NLC matrix elements versus the full-colour matrix elements, it might be

---

<sup>7</sup>We have considered two alternatives to using the colour-summed FC (or NLC) and LC matrix elements in Eq. (6). First, one could take only a single row ‘ $i$ ’ in the colour matrix in both the numerator and denominator [40, 46], i.e., the one corresponding to the LC colour ordering used to generate the LC unweighted events. While we have checked that this does give the correct FC (and NLC) cross section, the variance in the reweight factors is enormous, resulting in poor overall performance. Moreover, it yields a sizable fraction of negatively weighted events, since the numerator is no longer positive definite and is therefore not a viable option. The second alternative is to treat colour similarly to helicity; that is, assign to each external particle an explicit colour and/or anti-colour, weighted by their relative contribution to the LC matrix elements, and compute the numerator and denominator in the reweight factor only for that colour assignment. While this is guaranteed to result in positive reweight factors, we have found that the variance among these factors is much larger compared to summing over all colours, which again reduces the performance in the secondary unweighting step.

<sup>8</sup>In principle one does not need to consider the largest reweight factor(s) encountered (and therefore improve the efficiency because  $r_{\max}$  will be smaller) as long as the combined contribution one is neglecting is (well) within the statistical uncertainty of the event sample.



less computationally intensive to first reweight and unweight the LC events to NLC accuracy, and after that reweight them to full-colour using  $r^{\text{NLC} \rightarrow \text{FC}} = r^{\text{LC} \rightarrow \text{FC}} / r^{\text{LC} \rightarrow \text{NLC}}$ , and perform a tertiary unweighting step, since this might significantly reduce the number of events for which the full-colour matrix elements need to be evaluated. Since this depends strongly on the evaluation time and therefore on the details of the implementation of the NLC and full-colour matrix elements, which we have not fully optimised, we will only discuss the distribution of the  $\text{NLC} \rightarrow \text{FC}$  reweight factors in this work, and leave a full assessment and viability of this three-step approach to future studies.

### 3 Results

#### 3.1 Setup

In order to test our approach we consider multi-parton production in QCD both at a fixed collider energy and with a more realistic setup including parton luminosities. In both setups we include processes up to 7 partons in the final state. We consider processes with only gluons, processes with one quark line, and processes with 2 quark lines. For the latter, we consider both same- and different-flavour quarks, see the first column of Tab. 3.1 for the complete list of processes considered. For each of these flavour configurations, we consider all the distinct colour orderings contributing. We have listed the number of them in columns 2-7 of Tab. 3.1. As can be seen, the contributing number of distinct colour orderings is rather modest, even for high-multiplicity processes. This is because at high multiplicities there are more identical final-state particles, cancelling the factorial growth in the number of colour orderings. To be able to investigate the performance of our method in detail, each possible contribution is kept separate: we do not sum over quark flavours, nor combine different colour orderings in the integration. We treat each element in the sum of the r.h.s. of Eq. (3) as a separate integral for which we sample the same number of phase-space points and generate the same number of (unweighted) events. Note that in practical applications, this is not optimal, since one would like to compute channels that have a large contribution to the cross section with a higher accuracy than channels that have a smaller contribution.

In each of the channels, we use  $640 \times 10^3$  phase-space points (that pass the generation cuts) to setup the importance-sampling grids. After this, the grids are kept fixed and  $6.4 \times 10^6$  points (passing the generation cuts) are used to compute the phase-space integral, and determine the maximum weight for the (primary) unweighting. Instead of using a single maximum weight, we follow the procedure outlined in Ref. [47] to form a phase-space dependent upper bounding envelope<sup>9</sup>. To assess the efficiency of the integration methods, for each of the channels, we investigate the relative Monte Carlo uncertainties of the cross section. More importantly, we also investigate the unweighting efficiency for the generation of events, defined as

$$\epsilon_1 = \frac{N}{\tilde{N}}, \quad (8)$$

where  $N = 100$  is the number of unweighted events generated and  $\tilde{N}$  is the total number of phase-space points (that pass the cuts) tried to generate these  $N$  unweighted events. For each of the

---

<sup>9</sup>We have made various small changes to the method introduced in Ref. [47], of which the most important one is a more aggressive increase in the upper bound: following the notation of Ref. [47], if  $\bar{f} > \prod_{k=1}^n u^k(z_k)$ , we increase each  $u^k(z_k)$  by

$$f = \min \left( \frac{\bar{f}}{\prod_{k=1}^n u^k(z_k)}, 2 \right)^{1/n}.$$

This results in a faster convergence to a stable upper bound.

process	$n = 2$	$n = 3$	$n = 4$	$n = 5$	$n = 6$	$n = 7$
$gg \rightarrow n g$	2	2	3	3	4	4
$gg \rightarrow d\bar{d} + (n-2)g$	1	2	4	6	9	12
$\bar{d}g \rightarrow \bar{d} + (n-1)g$	2	3	4	5	6	7
$\bar{d}d \rightarrow n g$	1	1	1	1	1	1
$gg \rightarrow d\bar{d}d\bar{d} + (n-4)g$	-	-	2	4	11	18
$dg \rightarrow dd\bar{d} + (n-3)g$	-	2	6	12	20	30
$d\bar{d} \rightarrow d\bar{d} + (n-2)g$	2	3	5	6	8	9
$dd \rightarrow dd + (n-2)g$	1	1	2	2	3	3
$gg \rightarrow d\bar{d}u\bar{u} + (n-4)g$	-	-	4	8	22	36
$dg \rightarrow du\bar{u} + (n-3)g$	-	4	12	24	40	60
$d\bar{d} \rightarrow u\bar{u} + (n-2)g$	2	3	5	6	8	9
$du \rightarrow du + (n-2)g$	2	2	4	4	6	6

Table 1: Number of distinct elements (“channels”) contributing to the sum in the r.h.s. of Eq. (3).

channels, this procedure is repeated  $4 \times 10$  times for each of the 4 distinct phase-space parametrisations and for 10 different random number seeds. The latter allows us to estimate the stability of the results and assess the (potential) sensitivity to statistical outliers.

To study the secondary unweighting efficiency, computed as the normalised sum of all the ratios of the weights

$$\epsilon_2 = \frac{1}{N} \sum_{i=1}^N \frac{r_i}{r_{\max}}, \quad (9)$$

we need larger event samples. Therefore, in each channel and for each of the 10 different random number seeds, we generate  $N = 100 \times 10^3$  unweighted events. This is done for only one of the integration methods, since the four phase-space parametrisations yield statistically equivalent event files. We reweight the unweighted events both to  $LC \rightarrow FC$  and  $LC \rightarrow NLC$ , with the latter subsequently reweighted to  $NLC \rightarrow FC$  accuracy<sup>10</sup>.

A few comments on the definition of LC and NLC accuracy are in order. Firstly, as already discussed in Sec. 2.1.1, in the case of the different-flavour two-quark line processes, the definition of LC is not strictly that of a leading-colour approximation. In particular, all the (distinct) elements on the diagonal of the colour matrix, defined in the fundamental representation, are included as separate channels. This includes terms that contribute only at NLC accuracy. Secondly, for the NLC approximation, for the all-gluon processes, we strictly truncate all contributions beyond the

<sup>10</sup>The  $NLC \rightarrow FC$  efficiency does not take into account the change in weight distribution after the  $LC \rightarrow NLC$  reweighting and unweighting, since we compute the reweight factor for *each* LC event generated, rather than a subset corresponding to the unweighted NLC events.

NLC accuracy. Hence they include all the terms which are proportional to  $N_C^{n+2}$  and  $N_C^n$  and nothing beyond that. On the other hand, for the processes with at least one quark line, we do not truncate all the contributions beyond NLC. That is, we perform the colour decomposition of the amplitudes using the fundamental basis, and as soon as a coefficient in the colour matrix contributes at NLC, we include the full-colour version of that coefficient in our calculation. We have found that for these processes this yields a NLC approximation closer to the FC result as compared to truncating the value of the coefficient to NLC accuracy.

In this work we consider two setups for the event generation:

**Fixed partonic collision energy** In this setup, we use a fixed partonic collision energy of  $\sqrt{s} = 1000$  GeV, without the inclusion of initial-state parton distribution functions. We apply generation cuts on the two-body invariants  $|2p_i \cdot p_j| \geq 900$  GeV<sup>2</sup>, where  $i \neq j$ , including both initial- and final-state particles, and for the strong coupling we use a fixed value of  $\alpha_s = 0.119$ .

**LHC collision at 14 TeV** In this more realistic setup, we consider LHC collisions at 14 TeV, using the NNPDF2.3NLO PDF set [48]. The value of the strong coupling is still kept fixed at  $\alpha_s = 0.119$ , and the factorisation scale is set equal to the  $Z$ -boson mass. As generation cuts, we select events that have all final-state partons at a minimum transverse momentum of  $p_T > 30$  GeV, a maximum (absolute) rapidity of  $|y| < 6.0$  and a minimum separation between them of  $\Delta R > 0.4$ .

Except for the largest multiplicities considered, we have checked that the cross sections obtained with the setups above agree within statistical uncertainties with known results.

### 3.2 Numerical results for fixed partonic collision energy

In the left-hand plot of Fig. 2 we present the unweighting efficiencies,  $\epsilon_1$ , for the generation of LC events for the all-gluon processes. Processes with 2 up to 7 final-state gluons are considered. The four separate insets correspond to the (up to) four distinct colour orderings that need to be considered at LC accuracy, with the explicit colour ordering expressed in a string in the insets, using  $a$  and  $b$  for the labels of the right- and left-incoming partons and  $1, 2, \dots, n$  for the labels of the  $n$  outgoing partons. The various colours correspond to the phase-space parametrisations used: red for the Haag method, blue for the t-channel, and green for the gen2→3 parametrisation<sup>11</sup>. Since we have considered 10 different random seeds for each setup, we include vertical bars through the dots, showing the (barely visible) envelope of the 10 unweighting efficiencies obtained.

As expected, irrespective of the colour ordering and the phase-space parametrisation, the unweighting efficiency is much higher at low multiplicities compared to when more particles are produced in the final state. The differences between the colour orderings are not significant for the t-channel and the gen2→3 parametrisations, being above 50% for  $gg \rightarrow 2g$  and decreasing to the (several) per-mille level for  $gg \rightarrow 7g$ . With the exception of the  $n = 2$  and  $n = 3$  multiplicities, the gen2→3 method yields slightly larger efficiencies than the t-channel parametrisation. On the other hand, the Haag method behaves quite differently for each of the colour orderings. This method is designed to generate the phase-space density according to the all-gluon MHV matrix elements, and works particularly well for the  $(ab12\dots n)$  colour ordering, where all the final-state gluons are adjacent in the colour ordering. Indeed, for that case, Haag outperforms the other two methods by about an order of magnitude. For the  $(a1b2\dots n)$ , i.e., where one of the final-state gluons is separated from the others, the behaviour is worse: the efficiency of the Haag method is significantly lower than

<sup>11</sup>As discussed in Sec. 2.1.2, the  $p_T$ -based generator cannot be used for collisions at fixed partonic energy.

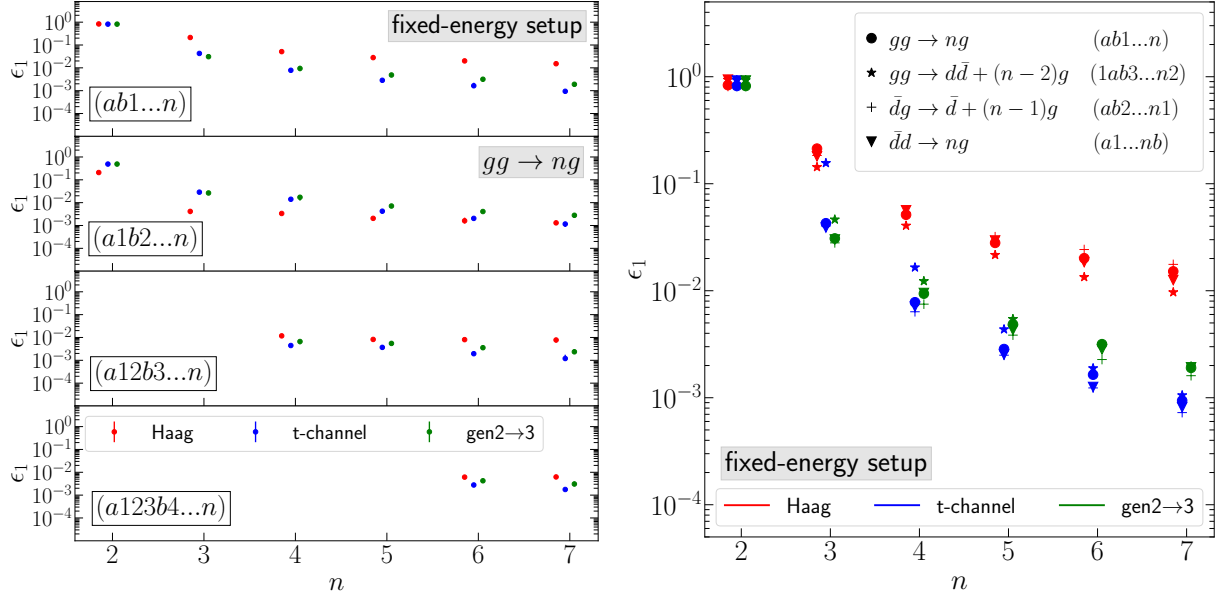


Figure 2: Unweighting efficiency,  $\epsilon_1$ , for the phase-space integration for the  $gg \rightarrow ng$  process (left plot), using the LC approximation of the integrand, for  $n = 2$  to  $n = 7$  number of final-state partons, the three integration methods and for all the non-equivalent colour orderings. In the right-hand plot we show  $\epsilon_1$  also for the process with one  $q\bar{q}$  pair, for the colour ordering in which all final-state gluons are adjacent. Both plots show the fixed partonic collision energy setup.

the other two parametrisations, in particular for moderate multiplicities. For the other two distinct colour orderings, Haag is slightly more efficient than the t-channel and gen2→3 methods, but still not as good as for the  $(ab12\dots n)$  ordering. The reason why the  $(ab12\dots n)$  colour ordering works most efficient with Haag is that for this configuration, all the final-state partons are constructed with antenna blocks [18], while in particular for  $(a1b2\dots n)$ , the momentum of gluon 1 is not generated according to an antenna block.

Similarly to what can be observed for the all-gluon processes in the left-hand plot of Fig. 2, we can see in the right-hand plot for the processes including one quark line. In the latter plot, we only consider the colour ordering where all final-state gluons are adjacent, and thus Haag is expected to be most optimal. Indeed, this is also what can be observed. Haag outperforms the other two phase-space parametrisations for all process types by a rather significant margin. However, we have checked that this is not the case for most of the other colour orderings one must consider, and the behaviour in this respect for the one-quark-line processes is very similar to the all-gluon process, discussed above.

In Fig. 3 we present the secondary (and tertiary) unweighting efficiencies,  $\epsilon_2$ , for the  $gg \rightarrow ng$  process as a function of  $n$ . Similarly to the left-hand plot of Fig. 2, we consider all the (up to) four distinct colour orderings. In cyan dots, we show the efficiency for the  $LC \rightarrow FC$  reweighting, in magenta the  $LC \rightarrow NLC$  efficiency and in black the (tertiary)  $NLC \rightarrow FC$  unweighting efficiency, and, as before, the vertical bars cover the extrema among the unweighting efficiencies obtained from the 10 independent samples produced.

As expected, the  $\epsilon_2$  measure is exactly equal to one for  $n = 2$  and  $n = 3$  in the all-gluon processes, because the beyond-LC contributions only result in an overall shift by the factor  $(1 - 1/N_C^2)$ . Starting

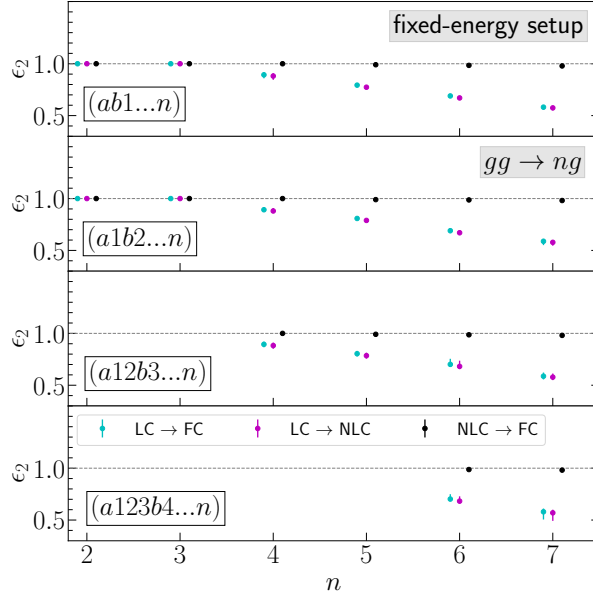


Figure 3: Secondary and tertiary unweighting efficiencies,  $\epsilon_2$ , for the all-gluon processes,  $gg \rightarrow ng$ , obtained after reweighting the LC to NLC and to FC, and the NLC to FC as a function of the gluon multiplicity  $n$ , for the fixed partonic energy setup.

from  $n = 4$ , this is no longer the case and both reweighting factors  $r^{\text{LC} \rightarrow \text{NLC}}$  and  $r^{\text{LC} \rightarrow \text{FC}}$ , as well as the tertiary reweighting factor  $r^{\text{NLC} \rightarrow \text{FC}}$  gain dependence on the kinematics of the event being reweighted. Increasing the multiplicity to  $n = 7$ , the variance in the factors increases, resulting in reduced efficiencies, but at all multiplicities considered, the secondary unweighting efficiencies  $\text{LC} \rightarrow \text{NLC}$  and  $\text{LC} \rightarrow \text{FC}$  remain above 50%, for all colour orderings. It should not come as a surprise that there is no large dependence on the colour ordering here: in the denominator of the reweight factors, Eq. 6, all colour orderings are summed over. Hence, the only dependence on the colour ordering comes through the kinematics of the generated LC event. In general, the  $\text{LC} \rightarrow \text{NLC}$  reweighting results in a slightly larger efficiency than the direct  $\text{LC} \rightarrow \text{FC}$  reweighting. And, the unweighting efficiency for  $\text{NLC} \rightarrow \text{FC}$  is always greater than 95%. This is a positive sign that an efficient three-step approach is possible: (1) generate LC unweighted events, (2) reweight and unweight those events to NLC accuracy, and (3) only then reweight (and unweight) the remaining events to FC accuracy. The outcome of this approach depends on the details of the implementation: not only the efficiencies, but also the timing (and potentially memory usage) of the LC, NLC and FC matrix elements determine if this three-step strategy is viable in practice. Since our implementations are not fully optimised, we refrain from making any claims here and leave it for future studies.

From this simplified setup, i.e., fixed partonic collision energy and generation cuts on all the two-particle invariants, we can conclude that our approach of generating unweighted LC events first, and only then reweighting them (and unweighting again) to FC (or NLC) accuracy, is viable. However, this setup is very much an ideal case. In particular, the Haag integrator is known to behave rather well when cuts are applied on the two-body invariants and not on the more commonly used kinematical variables at LHC, such as transverse momentum, rapidity and angular separation. We will study the latter in more detail in the next section.

### 3.3 Numerical results for the LHC setup

#### Generation of LC events

In this more realistic setup with included parton luminosities, we can see in Fig. 4, that the overall behaviour of the unweighting efficiencies in generating the LC events is rather similar to the fixed partonic collision energy results. In this figure, where we present exactly the same results as in Fig. 2, but for the LHC setup, we have now also included the results for the  $p_T$ -based phase-space parametrisation in yellow. For all the results presented here, this method has a worse performance than the other three parametrisations. This is not surprising: this method does not have any integration variables directly aligned with the peaks in the LC matrix elements, resulting in a poorer adaptation of the importance sampling towards the integrand. However, this is rather specific to integrating single colour orderings at a time. If one would integrate directly FC matrix elements (or multiple colour orderings together) the advantages of using Haag, t-channel or gen2→3 parametrisation are greatly reduced, while the  $p_T$ -based one would be less affected.

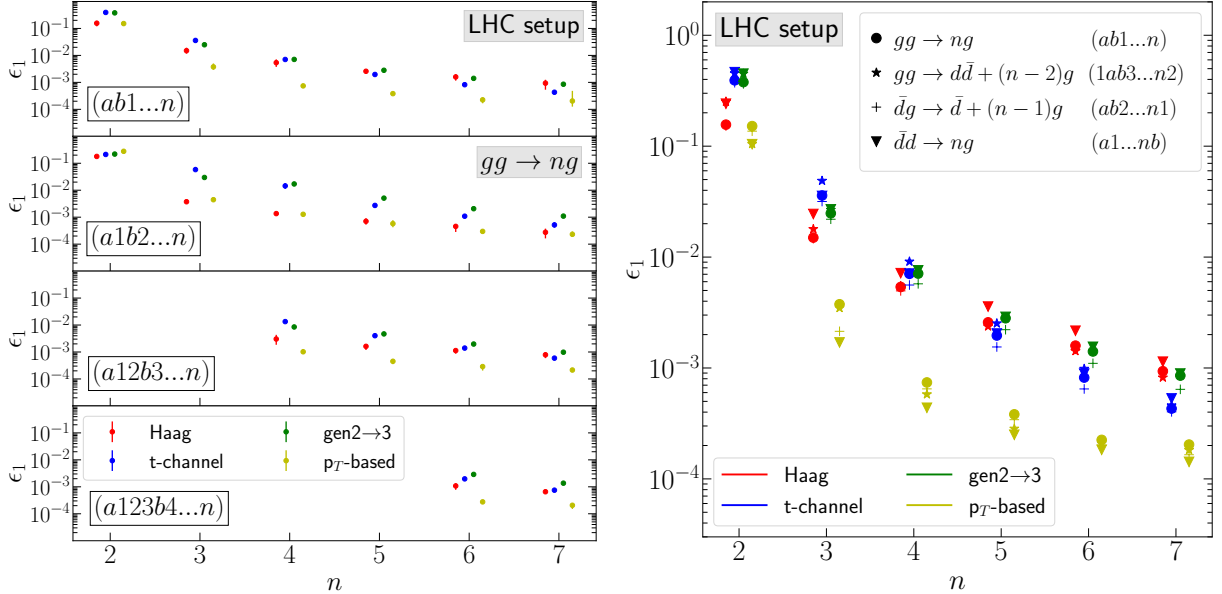


Figure 4: Unweighting efficiency,  $\epsilon_1$ , for the phase-space integration for the  $gg \rightarrow ng$  processes (left plot), using the LC approximation of the integrand, for the number of final-state partons  $n = 2$  to  $n = 7$ , the four integration methods and for all the non-equivalent colour orderings. In the right-hand plot we show the  $\epsilon_1$  measure also for the processes with one  $q\bar{q}$  pair, for the colour ordering in which all final-state gluons are adjacent. Both plots show the LHC setup.

By comparing the unweighting efficiencies for the LHC setup (Fig. 4) with the ones for the fixed partonic collision energy (Fig. 2), we notice a slightly poorer overall performance. This comes as no surprise, since there are two extra integration variables (the Bjorken  $x$ 's) and slightly more complicated phase-space cuts in the LHC setup, the variance among the phase-space points increases somewhat, resulting in the decreased efficiency. This is particularly noticeable for the Haag parametrisation, that performs considerably worse with cuts on the  $p_T$ ,  $\eta$  and  $\Delta R$  as compared to the two-body invariants in the fixed partonic collision energy setup. The main reason is that these cuts impact the integration boundaries of the variables used in the Haag integration in a complex

manner, meaning that optimisation is difficult, resulting in many generated phase-space points not passing these cuts. Even though these points are not included in the computation of the unweighting efficiencies, they do impact the setup of the importance sampling grids, potentially increasing the variance among the points passing the cuts.

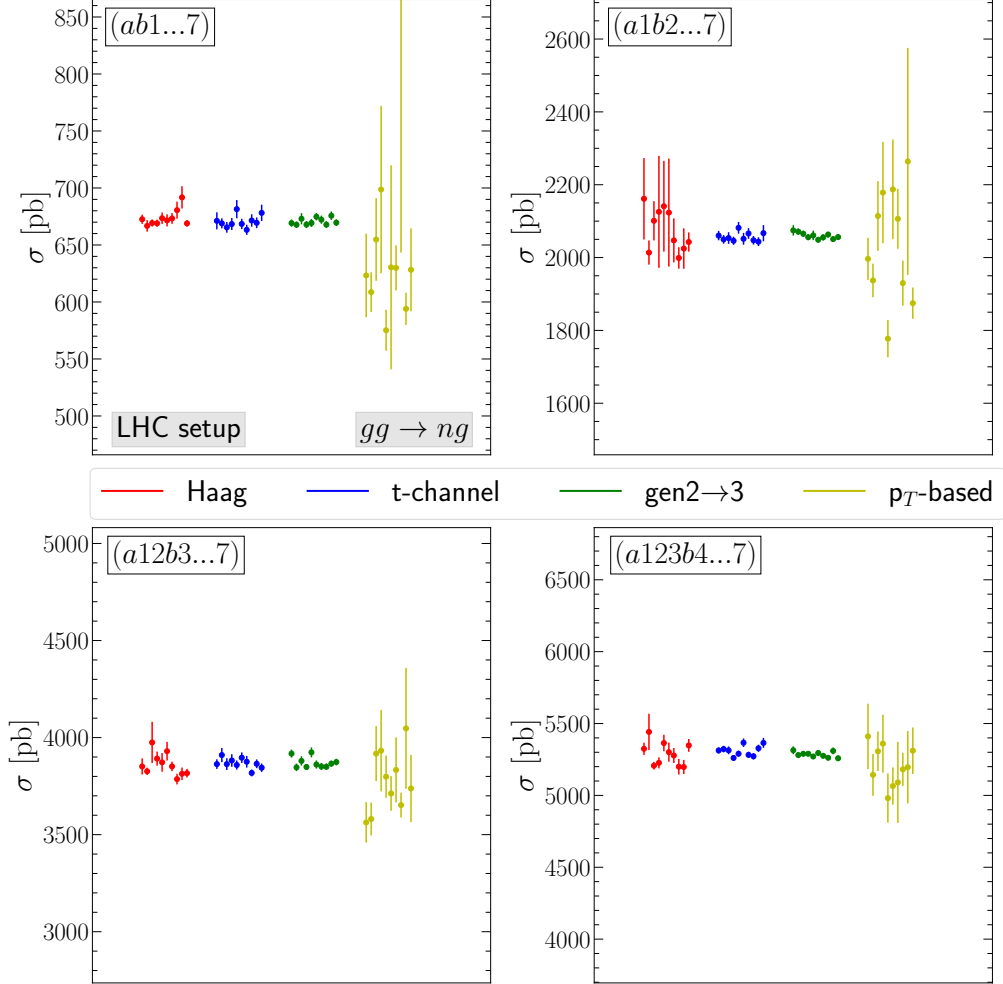


Figure 5: Cross section (in pb) for the  $gg \rightarrow 7g$  process for the four distinct colour orderings and the four different phase-space parametrisations for the LHC setup. Each setup is repeated 10 times with a different random number seed, resulting in the 10 points per integration method. The vertical bars indicate the statistical Monte Carlo uncertainty on the cross sections. The cross sections include a factor  $7!$ , corresponding to the final-state symmetry factor.

The values for the unweighting efficiencies are highly correlated with the statistical uncertainties obtained from the Monte Carlo phase-space integration, presented in Fig. 5. In this figure, the LC cross section (in units of pb) for the  $gg \rightarrow 7g$  process is shown. Results are separated in the four distinct colour orderings, and repeated for the four phase-space parametrisations considered. Moreover, each complete setup is repeated 10 times with different random number seeds. As can be seen, all the obtained cross sections among the  $4 \times 10$  runs are compatible within their statistical uncertainties (the  $1\sigma$  statistical errors are given by the vertical bars). Moreover, the uncertainties

obtained and the spread among the cross sections are the smallest with the  $\text{gen2} \rightarrow 3$  parametrisation. This is compatible with the fact that this setup has the largest unweighting efficiency. Similarly, the  $p_T$ -based method shows the largest spread and uncertainties in the cross section, resulting in the smallest unweighting efficiency, as discussed above.

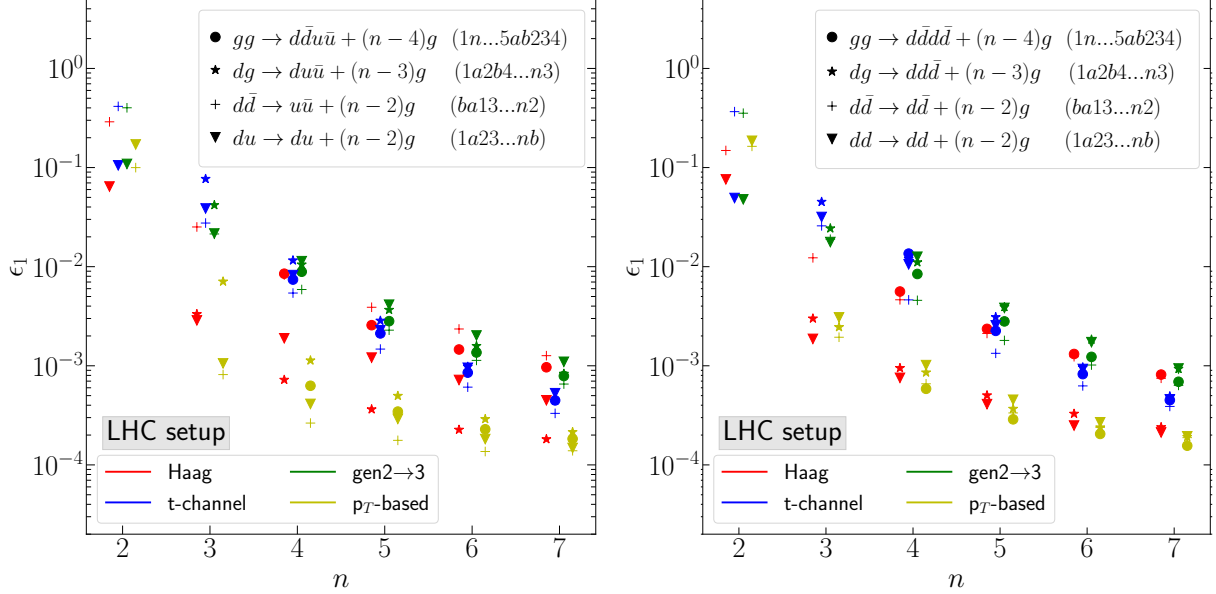


Figure 6: Unweighting efficiency,  $\epsilon_1$ , for the phase-space integration for the two quark-pair process with different flavours (left plot) and same flavours (right plot) for the LHC setup, using the LC approximation of the integrand, for the number of final-state partons  $n = 2$  to  $n = 7$ , using the four integration methods. Only a single colour ordering is considered for each of the flavour channels, specified in the legend.

The main features of the results for the unweighting efficiencies for the generation of the LC events obtained for the  $gg \rightarrow ng$ ,  $gg \rightarrow d\bar{d} + (n-2)g$ ,  $\bar{d}g \rightarrow \bar{d} + (n-1)g$ , and  $\bar{d}d \rightarrow ng$  processes translate to the processes with two quark lines. In Fig. 6 we present these values for the different-flavour (left plot) and same-flavour (right plot) quark lines. In these plots, only one of the colour orderings is considered (one of orderings with most of the final-state gluons adjacent), but the results for the t-channel,  $\text{gen2} \rightarrow 3$ , and  $p_T$ -based parametrisations are representative for the other colour orderings. For the Haag method, however, similarly to the all-gluon process, see left-hand plot of Fig. 4, the colour ordering with all final-state gluons adjacent works best, and for the other orderings (not-shown), Haag performs somewhat worse compared to the other methods.

From the results in these figures, we can conclude that, overall, the  $\text{gen2} \rightarrow 3$  method behaves excellently (with the t-channel a close second) for all processes, colour orderings and multiplicities, with unweighting efficiencies at (or above) the per-mille level, even for  $2 \rightarrow 7$  processes.

### Reweighting the LC events

The main results for the secondary (and tertiary) unweighting efficiencies,  $\epsilon_2$ , are summarised in Fig. 7. In this figure, we have focused on the highest multiplicity that we have considered,  $n = 7$ , and, for each process, have selected one or two representative colour orderings. In this figure,  $\epsilon_2$  is



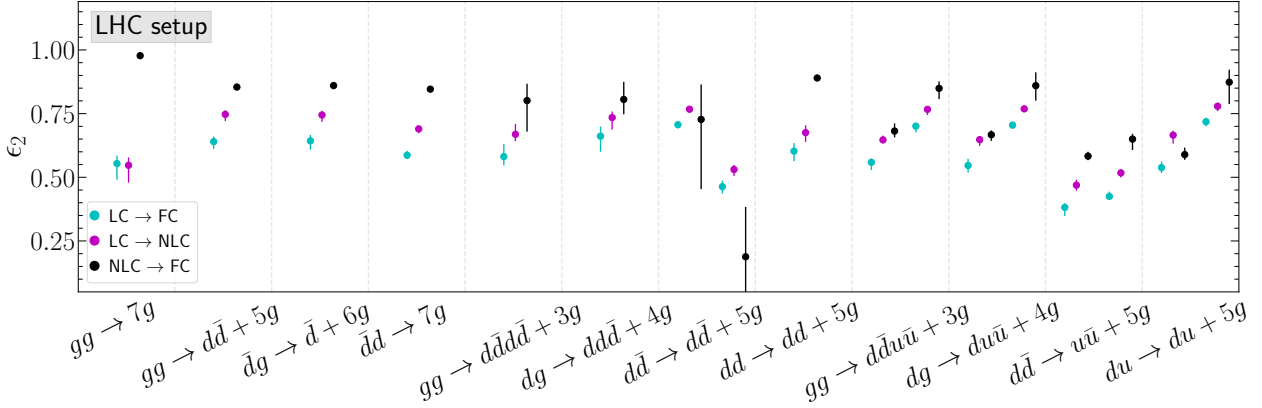


Figure 7: Secondary (and tertiary) unweighting efficiencies,  $\epsilon_2$ , for all the  $2 \rightarrow 7$  processes for various flavours, for one or two representative colour orderings, for the LHC setup.

represented by the cyan, magenta and black dots for the reweighting of  $LC \rightarrow FC$ ,  $LC \rightarrow NLC$ , and  $NLC \rightarrow FC$ , respectively.

In the first column of this figure, the  $gg \rightarrow 7g$  process is shown. The unweighting efficiencies  $LC \rightarrow FC$  and  $LC \rightarrow NLC$  are about 50% for this channel, with some minor variations for the 10 different random seeds, represented by the small vertical bars on the dots. The tertiary unweighting efficiency coming from the  $NLC \rightarrow FC$  reweighting is rather large, above 95%. The secondary (and tertiary) unweighting efficiencies,  $\epsilon_2$ , for the other multiplicities and colour orderings for the all-gluon processes are shown in Fig. 8. We find similar results as for the fixed partonic collision energy (Fig. 3). Even though the kinematics of the events in the fixed partonic collision energy setup differ from those in the LHC setup, the reweighting factors are similar and the secondary (and tertiary) unweighting efficiencies are very close in value.

In Fig. 9 we show the actual weight distributions corresponding to these unweighting efficiencies for the all-gluon processes. In the top row, the weight distributions of the  $r^{LC \rightarrow FC}$  and  $r^{LC \rightarrow NLC}$  reweight factors are shown in the darker and lighter lines, respectively, and in the bottom row the tertiary  $r^{NLC \rightarrow FC}$  reweight factor. The colours represent the different final-state multiplicities that we consider, and the colour ordering is specified in the subplots. For these plots, and any following plots that show the specific weight distributions, we group the events created with the 10 different random seeds together in one event file. Hence, each of the distributions shown in these figures are generated from  $10^6$  unweighted LC events.

As expected, the  $n = 2$  (blue) and  $n = 3$  (black) distributions are single peaks, located at  $r^{LC \rightarrow FC} = r^{LC \rightarrow NLC} = (N_C^2 - 1)/N_C^2$ , and  $r^{NLC \rightarrow FC} = 1$ , since the NLC contributions are an overall shift of the LC results for the four- and five-gluon amplitudes. For  $n = 4$  and above, the reweight factors are no longer constant over the phase space. Moreover, there are beyond-NLC contributions, such that  $r^{LC \rightarrow FC} \neq r^{LC \rightarrow NLC}$  in general. However, the two curves remain close to each other for all the multiplicities and colour orderings considered. Furthermore, these weight distributions remain very much peaked at  $(N_C^2 - 1)/N_C^2$ , with a somewhat increasing tail towards larger reweight factors at higher multiplicities. However, even for  $n = 7$ , they remain below about a factor two above the peak, which corresponds to the about 50% secondary unweighting efficiencies found for this multiplicity as depicted (by the cyan and magenta dots) in Fig. 8. Note also that by comparing the weight distributions for the up-to-four distinct colour orderings, they behave rather similarly. This

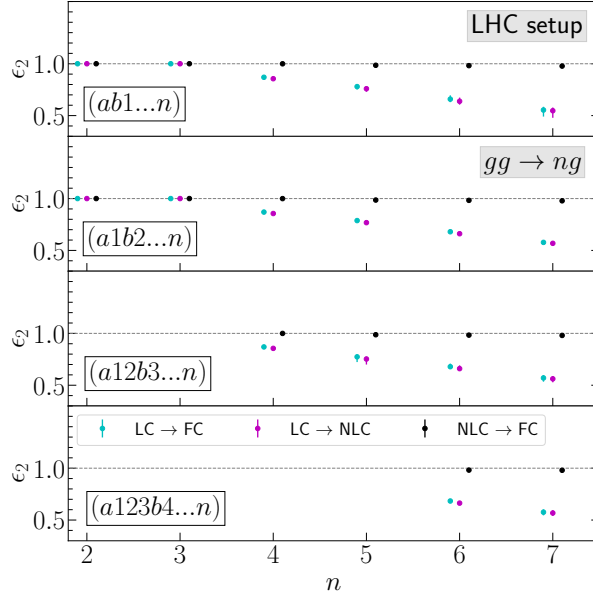


Figure 8: Secondary (and tertiary) unweighting efficiencies,  $\epsilon_2$ , for the reweighting of the LC events for the  $gg \rightarrow ng$  process, for  $n = 2$  to  $n = 7$  number of final-state partons, and for all the non-equivalent colour orderings, for the LHC setup.

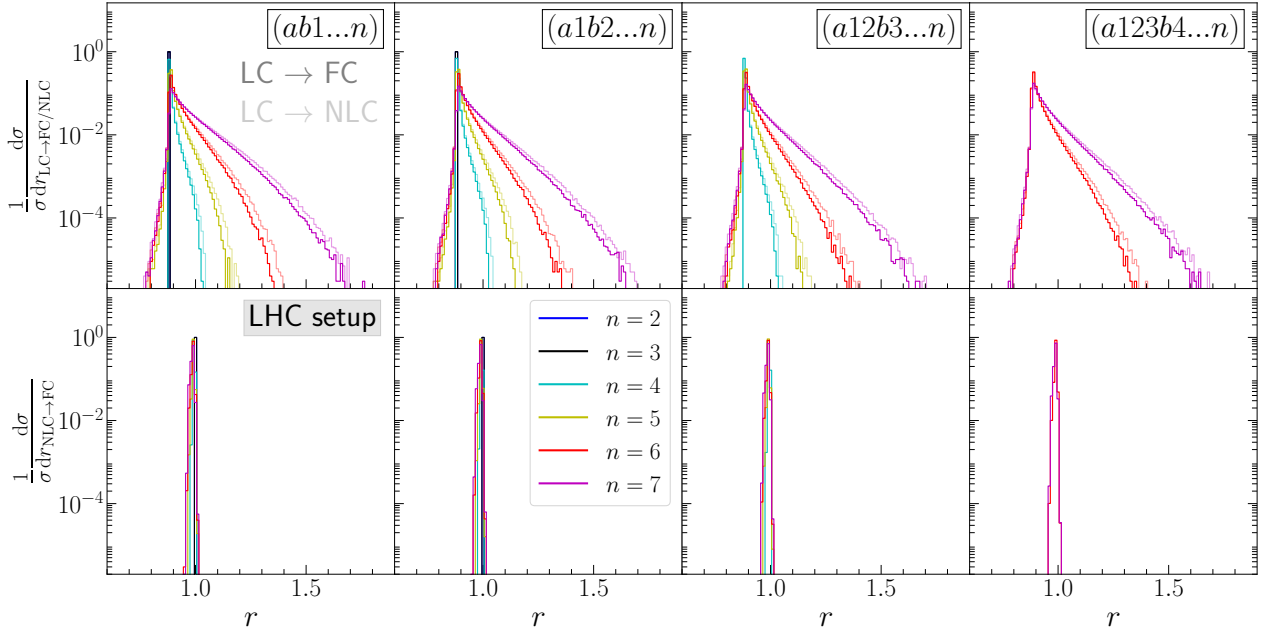


Figure 9: Weight distributions for the reweight factors  $r^{\text{LC} \rightarrow \text{FC}}$  and  $r^{\text{LC} \rightarrow \text{NLC}}$  in the top row and  $r^{\text{NLC} \rightarrow \text{FC}}$  in the bottom row for the all-gluon processes, for the various distinct colour orderings in the four columns, for the LHC setup. The colours represent the different final-state multiplicities.

is because the colour ordering itself does not enter the actual reweight factors directly; only through the kinematics of the unweighted LC events, the colour ordering plays a role in the reweighting. The very large tertiary unweighting efficiencies,  $> 95\%$ , correspond to the very narrow peaks in the  $\text{NLC} \rightarrow \text{FC}$  weight distributions (lower row). They are peaked exactly at 1 for the low to medium multiplicities, but shift to a few percent below 1 for highest multiplicities considered.

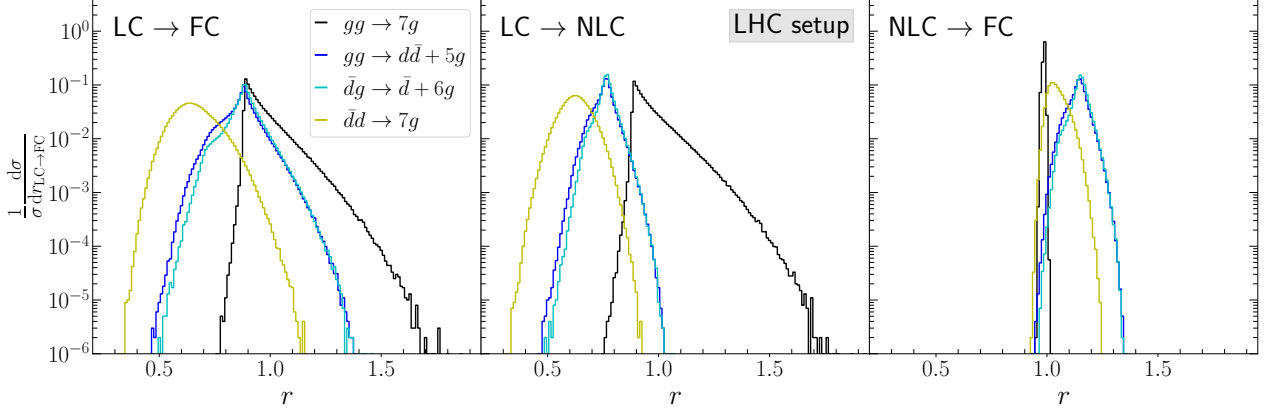


Figure 10: Weight distributions for the reweight factors  $r^{\text{LC} \rightarrow \text{FC}}$  and  $r^{\text{LC} \rightarrow \text{NLC}}$  and  $r^{\text{NLC} \rightarrow \text{FC}}$  for the  $gg \rightarrow 7g$  (black),  $gg \rightarrow d\bar{d} + 5g$  (blue),  $g\bar{d} \rightarrow \bar{d} + 6g$  (cyan),  $\bar{d}d \rightarrow 7g$  (yellow) processes, for the LHC setup. For each, one (representative) colour order is chosen.

In Fig. 10 we compare the weight distributions for the reweight factors for the  $n = 7$  all-gluon process (in black), with the one-quark-pair processes: in blue the  $gg \rightarrow d\bar{d} + 5g$  process, in cyan the  $g\bar{d} \rightarrow \bar{d} + 6g$  process, and in yellow the  $\bar{d}d \rightarrow 7g$  process. As expected, for the one-quark-line processes in which the quarks are not back-to-back, the peak in the  $\text{LC} \rightarrow \text{FC}$  reweighting is also located at  $(N_C^2 - 1)/N_C^2$ , with a narrower weight distribution than the all-gluon processes. On the other hand, for the  $\bar{d}d \rightarrow 7g$  process, the weight distribution is rather different. The peak is at a lower value and is much broader, especially close to the peak. We find that this is generally the case when the kinematics associated with the quark and anti-quark are back-to-back; a similar broader spectrum is obtained for the  $n = 4$   $gg \rightarrow d\bar{d}$  process (not shown), in which the quarks are also back-to-back. We have not investigated the mechanism behind this. Comparing the  $\text{LC} \rightarrow \text{FC}$  to the  $\text{LC} \rightarrow \text{NLC}$  weight distributions, we find that the  $\text{LC} \rightarrow \text{NLC}$  are considerably narrower, and not peaked at the same values, which is compensated for by the tertiary  $\text{NLC} \rightarrow \text{FC}$  reweight distributions. Consistent with these weight distributions, in the 2<sup>nd</sup> to 4<sup>th</sup> columns of Fig. 7 we observe that the secondary unweighting efficiencies are larger for the  $\text{LC} \rightarrow \text{FC}$  and  $\text{LC} \rightarrow \text{NLC}$  reweighting for the one-quark line processes than for the all-gluon process. On the other hand, the NLC approximation more closely matches the FC result for the all-gluon process, resulting in a narrow peak at 1 for the  $\text{NLC} \rightarrow \text{FC}$  reweight factors; for the one-quark-line processes the  $\text{NLC} \rightarrow \text{FC}$  weight distribution is wider, but still quite a bit narrower than for the  $\text{LC} \rightarrow \text{FC}$  (and  $\text{LC} \rightarrow \text{NLC}$ ), which confirms the larger tertiary than secondary unweighting efficiencies for these processes. For lower multiplicities (not shown) the weight distributions become considerably narrower, resulting in considerably larger secondary and tertiary unweighting efficiencies.

Before moving on to the two-quark-pair processes, in Fig. 11 we show the weight distribution for the  $\text{LC} \rightarrow \text{FC}$  reweight factors for the  $n = 5$  one-quark-line processes for each of the distinct colour orderings. Since the only way the colour ordering enters the weight distributions is through the

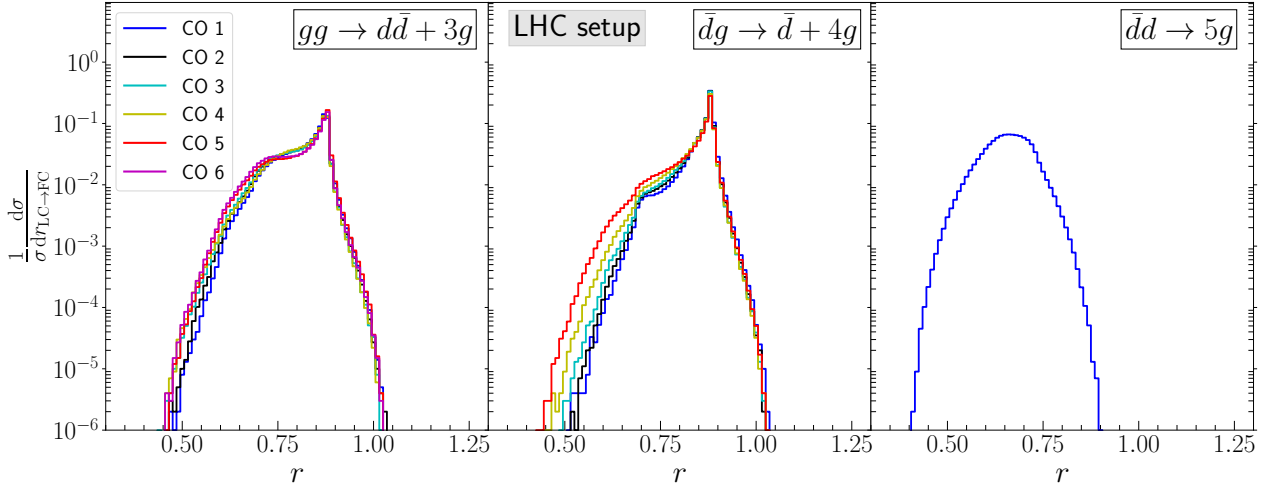


Figure 11: Weight distributions showing the colour ordering dependence for the  $\text{LC} \rightarrow \text{FC}$  reweight factors for the three one-quark-line processes, for the LHC setup.

kinematics of the unweighted LC events, it can be expected that the dependence of the distributions on the ordering is mild. Indeed, for both the  $gg \rightarrow d\bar{d} + 3g$  and  $g\bar{d} \rightarrow \bar{d} + 4g$  the difference is small, whereas for the  $d\bar{d} \rightarrow 5g$  process, only one distinct colour ordering needs to be considered because all final-state particles are identical gluons (see Tab. 3.1). We observe the same independence from the colour ordering also for other multiplicities and for the all-gluon processes; c.f. Fig. 7.

In general, for the two-quark-line processes the secondary unweighting efficiencies in the reweighting of the LC events to FC, we find unweighting efficiencies in the 50-70% range for the  $n = 7$  processes (lower multiplicities yield larger efficiencies), see Fig. 7. Just as in the one-quark-line case, the unweighting efficiencies for reweighting  $\text{LC} \rightarrow \text{NLC}$  are about 7-10 percent points higher than those for reweighting to FC. However, there is a significant variation in the secondary unweighting efficiencies among the different flavour assignments. Moreover, contrary to the all-gluon and the one-quark line processes, there is also a dependence in the efficiencies from the colour ordering in some of the processes. In the latter case, instead of showing a single representative colour ordering, we present two of them in Fig. 7. As discussed before, the colour ordering does not directly enter the reweighting, since both the numerator and denominator in Eq. (6) are summed over all colour orderings. It enters only through the kinematics of the events, which, in turn, is dominated by how the two quark pairs are ordered:

1. For processes that have a quark-anti-quark pair in the initial and in the final state, the ordering in which initial-state anti-quark is followed by the initial-state quark and the final-state quark is followed by the final-state anti-quark, e.g.  $(b \dots a 3 \dots 4)$  for the process  $d\bar{d} \rightarrow u\bar{u} + (n-2)g$ , has a larger secondary unweighting efficiency than the colour orderings where the initial-state anti-quark is followed by a final-state anti-quark and the final-state quark is followed by the initial-state quark, e.g.  $(3 \dots ab \dots 4)$ .
2. For different-flavour quark line processes, and as discussed in Sec. 2.1.1, we include all the elements on the diagonal of the colour matrix (in the fundamental basis) as part of our LC approximation, even though only half of them contribute at LC and the other half only at NLC accuracy. The channels for which the colour ordering contributes only at NLC (i.e., the

quark anti-quark pairs of the same flavours form a substring in the colour ordering—possibly with gluons in between) have a smaller secondary unweighting efficiency than channels that contribute at LC (i.e., the quark anti-quark pairs that form a substring in the colour ordering have different flavours).

These two general rules explain the differences observed in the secondary unweighting efficiencies for the two-quark-line processes: for processes  $gg \rightarrow d\bar{d}d\bar{d} + (n-4)g$ ,  $dg \rightarrow d\bar{d}d + (n-3)g$  and  $dd \rightarrow dd + (n-2)g$  we find hardly any variation among the contributing colour orderings and we show the results for only a single representative colour ordering; for the  $d\bar{d} \rightarrow d\bar{d} + (n-2)g$  process we have two representative sets of efficiencies due to point 1 above; for processes  $gg \rightarrow d\bar{d}u\bar{u} + (n-4)g$ ,  $dg \rightarrow du\bar{u} + (n-3)g$  and  $du \rightarrow du + (n-2)g$  we have two sets of efficiencies due to point 2 above; and, finally, points 1 and 2 both apply to the  $d\bar{d} \rightarrow u\bar{u} + (n-2)g$  processes. In the latter case, the points counteract each other, resulting in a single representative secondary unweighting efficiency (see the two similar efficiencies for this process in Fig. 7).

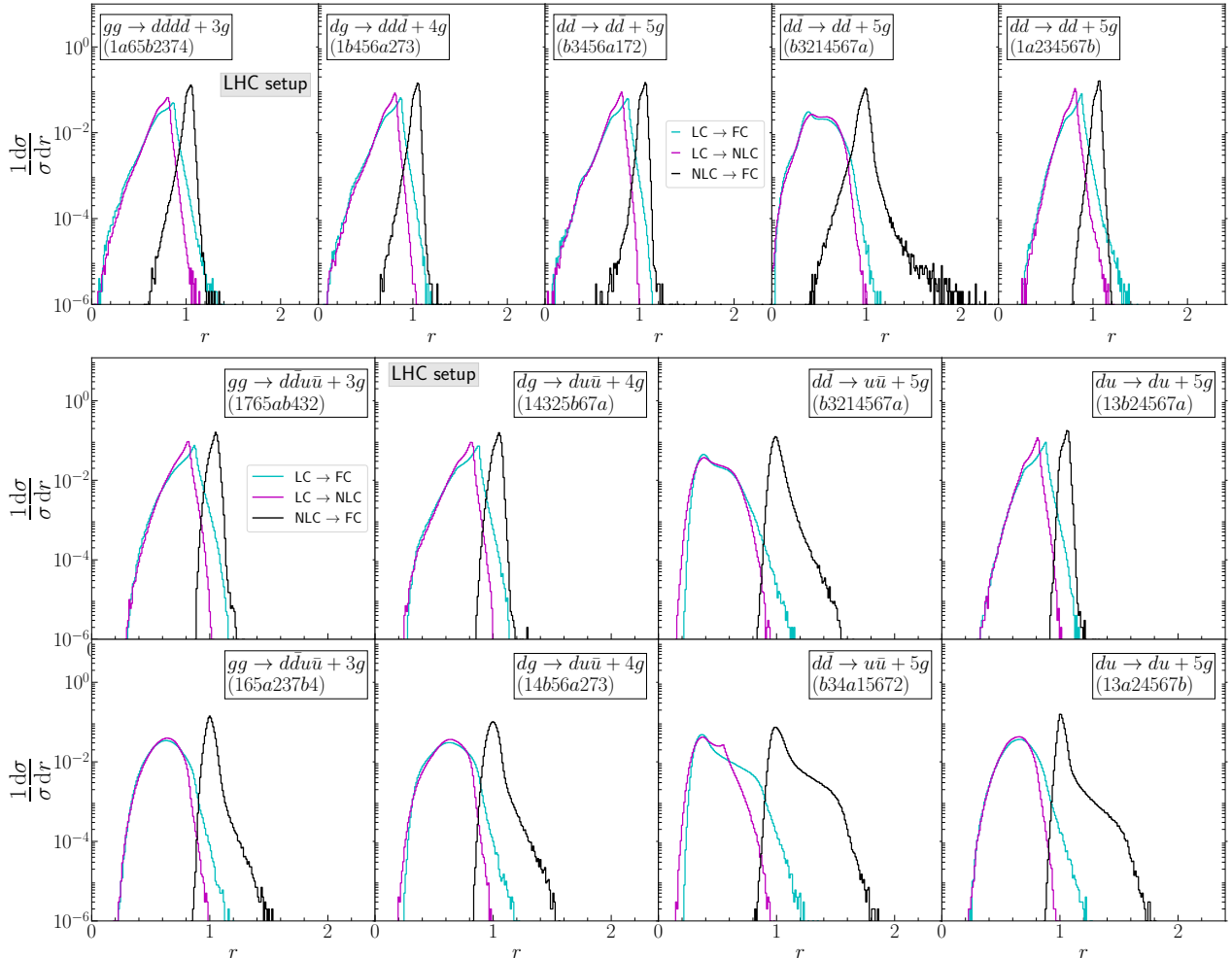


Figure 12: Weight distributions of the reweight factors for representative channels in the  $n = 7$  two-quark-line processes, for same-flavour processes (upper plot) and different-flavour processes (lower plot).

The differences in the secondary unweighting efficiencies can, of course, also be observed in the weight distributions for the reweight factors directly, see Fig. 12. In this figure the distributions correspond to the colour orderings for which the efficiencies are presented in Fig. 7. In the top row of this figure, the weight distributions for a representative channel for the four  $n = 7$  same-flavour two-quark-line processes are shown; for the  $d\bar{d} \rightarrow d\bar{d} + 5g$  process the two representative quark orderings, see point 1 above, are presented. In the lower plot, the different-flavour two-quark-line weight distributions for the reweighting are shown for both ways the quarks can be ordered, as discussed in point 2 above, with the upper row containing the ordering such that it contributes to LC, and the lower row such that it contributes to NLC. In cyan we show the weight distributions of the reweight factors in the LC  $\rightarrow$  FC reweighting, in magenta for the LC  $\rightarrow$  NLC reweighting and in black the NLC  $\rightarrow$  FC reweighting.

Let us focus on the LC  $\rightarrow$  FC and LC  $\rightarrow$  NLC reweighting first. As is clear from these plots, the weight distributions in subplots 1, 2, 3, and 5 in the upper plot, and 1, 2, and 4 in the upper row of the lower plot show nicely peaked distributions resulting in the larger secondary unweighting efficiencies. The 4th subplot in the upper plot and the 3rd subplot in the upper row of the lower plot show similar shaped distributions, confirming that the reduced secondary unweighting efficiency is indeed due to the ordering of the initial- and final-state (anti-)quarks. The main difference in the reweight factors for the same-flavour and different-flavour processes is that for the same-flavour processes, the distribution extends to much smaller values. Subplots 1, 2 and 4 in the lower row of the lower plot again show similar shape; these are obtained from events that were generated with a colour ordering that only contributes starting at NLC. The third subplot in the lower row of the lower figure has its own unique shape. As explained before, this flavour configuration is unique because it is obtained from an event file generated from a NLC colour ordering, but also has the initial-initial plus final-final (anti-)quark ordering.

In the three-step approach, reweighting LC  $\rightarrow$  NLC  $\rightarrow$  FC, we can see in Fig. 12 that the total rate of the NLC requires a shift to get to FC in some of the channels: when the LC  $\rightarrow$  FC and LC  $\rightarrow$  NLC distributions are very peaked, their peaks do not align, resulting in a NLC  $\rightarrow$  FC peak that is not located at 1. On the other hand when the weight distributions are broader, the NLC  $\rightarrow$  FC peak is located closer to 1.

For some of the same-flavour processes (upper plot in Fig. 12), both the LC  $\rightarrow$  FC and LC  $\rightarrow$  NLC reweight factors approach zero. Even though the absolute difference between these two reweight factors is very small in this region, the relative difference can be significant. Indeed, in the ratio of these factors, i.e., the NLC  $\rightarrow$  FC reweight factors, we observe a sizable tail towards larger factors. These runaway tails hamper the tertiary unweighting efficiency significantly. Given that we find several configurations with significantly lower tertiary reweighting efficiencies, and, in particular observe runaway tails at times, the reweighting (and unweighting) to an intermediate NLC accuracy does not appear to be most-efficient for these processes.

## General remarks

We end this section with a few remarks regarding the accuracy of first generating LC events, reweighting them to higher accuracy, and performing a secondary unweighting.

The first remark relates to the computation of  $r_{\max}$  used as maximum value against which the secondary unweighting is performed, see Eq. 7. Currently we estimate this channel-by-channel by taking the maximum value found in each event file generated. An alternative would be to take the maximum value in any of the events generated for a given process, irrespective of the colour ordering used to generate the individual event files. In general, the latter method would reduce the

unweighting efficiencies somewhat, but would not change the overall results presented here. On top of that, we believe that defining  $r_{\max}$  channel-by-channel, as we do, is more correct: even though each channel covers the full phase space, due to the different phase-space parametrisation and integrand, each channel covers the phase space differently. Phase-space regions for which  $r_{\max}$  is large can have a much smaller measure in some channels than others, effectively reducing the  $r_{\max}$  to use in practice. By keeping a separate  $r_{\max}$  in each channel, we take this effect into account.

Second, for our procedure to work, the LC approximation must fill the full phase space: it must not be the case that for a given phase-space region the LC matrix elements are zero (or very small) while the FC ones are non-zero. For the processes considered here there is indeed no sign of such phase-space regions: there are no runaway tails in the distributions of the reweight factors that hamper the secondary unweighting efficiencies: they all have a relatively sharp drop-off above which there are no events. This, together with the fact that the cross sections agree with known results within statistical uncertainties shows that we have obtained the correct FC results with our method.

On the other hand, for the NLC  $\rightarrow$  FC reweighting for the same-flavour two-quark-line processes, these phase-space regions do exist. For some channels we indeed notice that there are phase-space regions in which the NLC is (close to) zero, while the FC is not, resulting in a large variation in the tertiary unweighting efficiencies among the 10 different random seeds used for each channel. Moreover, one can also directly observe this in the weight distributions for the NLC  $\rightarrow$  FC reweight factors for these processes. This means that one should not perform a three-step approach, but rather reweight LC directly to FC, where this problem does not arise. Alternatively, it might be possible to include some terms beyond the NLC accuracy in our NLC approximation to move it closer to the FC and by doing so removing the phase-space region where the NLC approximation is close to zero.

## 4 Conclusions and Outlook

In this work we have presented a two-step approach to event generation at leading order in the perturbative expansion. In a first step we use a fast approximation of the integrand to perform the phase-space integration and generate unweighted events. We use (a small number of) single colour-ordered matrix elements as the approximation; each single colour-ordered amplitude squared forms its own channel and can be integrated in parallel. Since the integrands are very fast to evaluate, and also have a relatively simple phase-space dependence, the generation of these events is fast and the unweighting can be performed at high efficiency: even for  $2 \rightarrow 7$  processes, we find efficiencies at or above the per-mille level with the gen2 $\rightarrow$ 3 phase-space parametrisation in all the integration channels.

As a second step, the LC-accurate events are reweighted to full-colour, and unweighted again. Since phase-space dependence in the needed reweight factors is small, secondary unweighting efficiencies are typically well above 50%, even at the highest multiplicities we have considered in this work. In practice this means that in order to generate a certain number of unweighted events, for less than twice that number the slow, full-colour matrix elements need to be evaluated. Moreover, this reweighting procedure can be trivially parallelised, since each LC event can be reweighted independently.

Compared to the traditional approach of integrating the full-colour matrix elements directly over the phase space (either with or without a Monte Carlo sum over colours), our method yields a double improvement. Not only is the number of phase-space points for which the full-colour matrix elements need to be evaluated much smaller in the generation of a given number of unweighted events, also

the phase-space integration itself is more efficient since the LC matrix elements for a given colour ordering have a much simpler dependence on the phase space than the full-colour ones.

We plan to apply our method also to processes including massive QCD particles such as top quarks or bottom quarks and electroweak bosons in the future. We do not foresee any problems for the inclusion of masses; the inclusion of non-coloured particles might impose more difficulties. In particular, our phase-space generation for the LC events is optimised for a specific colour ordering of all the produced particles—non-coloured particles do not fit neatly into this picture, and might require several more integration channels for efficient event generation and unweighting. On the other hand, electroweak particles do not play any special role in the reweighting of the LC events to FC, and so the second step in our approach should not be seriously affected.

It would be interesting to investigate if the method of using several consecutive unweighting steps can be applied more broadly. For example, starting from an unweighted LO event file, could the events be efficiently reweighted to generate (part of) an NLO-accurate event file? In particular, the S-events in MC@NLO [49] or MC@NLO- $\Delta$  [50] matching, or the  $\overline{B}$  function in the POWHEG method [51], have the same kinematics as the LO contributions; they could be suitable candidates for studies in this direction.

## Acknowledgements

This work was supported by the Swedish Research Council under contract numbers 201605996 and 202004423. The work of T.V. is supported by the Swedish Research Council, project number VR:2023-00221.

## References

- [1] G. P. Lepage, *A New Algorithm for Adaptive Multidimensional Integration*, *J. Comput. Phys.* **27** (1978) 192.
- [2] G. P. Lepage, *Adaptive multidimensional integration: VEGAS enhanced*, *J. Comput. Phys.* **439** (2021) 110386, [2009.05112].
- [3] A. van Hameren, *PARNI for importance sampling and density estimation*, *Acta Phys. Polon. B* **40** (2009) 259–272, [0710.2448].
- [4] R. Kleiss and R. Pittau, *Weight optimization in multichannel Monte Carlo*, *Comput. Phys. Commun.* **83** (1994) 141–146, [hep-ph/9405257].
- [5] T. Ohl, *Vegas revisited: Adaptive Monte Carlo integration beyond factorization*, *Comput. Phys. Commun.* **120** (1999) 13–19, [hep-ph/9806432].
- [6] F. Maltoni and T. Stelzer, *MadEvent: Automatic event generation with MadGraph*, *JHEP* **02** (2003) 027, [hep-ph/0208156].
- [7] C. G. Papadopoulos, *PHEGAS: A Phase space generator for automatic cross-section computation*, *Comput. Phys. Commun.* **137** (2001) 247–254, [hep-ph/0007335].
- [8] F. Krauss, R. Kuhn and G. Soff, *AMEGIC++ 1.0: A Matrix element generator in C++*, *JHEP* **02** (2002) 044, [hep-ph/0109036].



- [9] W. Kilian, T. Ohl and J. Reuter, *WHIZARD: Simulating Multi-Particle Processes at LHC and ILC*, *Eur. Phys. J. C* **71** (2011) 1742, [0708.4233].
- [10] T. Gleisberg and S. Hoeche, *Comix, a new matrix element generator*, *JHEP* **12** (2008) 039, [0808.3674].
- [11] J. Alwall, R. Frederix, S. Frixione, V. Hirschi, F. Maltoni, O. Mattelaer et al., *The automated computation of tree-level and next-to-leading order differential cross sections, and their matching to parton shower simulations*, *JHEP* **07** (2014) 079, [1405.0301].
- [12] SHERPA collaboration, E. Bothmann et al., *Event Generation with Sherpa 2.2*, *SciPost Phys.* **7** (2019) 034, [1905.09127].
- [13] R. Kleiss, W. J. Stirling and S. D. Ellis, *A New Monte Carlo Treatment of Multiparticle Phase Space at High-energies*, *Comput. Phys. Commun.* **40** (1986) 359.
- [14] S. Plätzer, *RAMBO on diet*, 1308.2922.
- [15] E. Byckling and K. Kajantie, *Reductions of the phase-space integral in terms of simpler processes*, *Phys. Rev.* **187** (1969) 2008–2016.
- [16] E. Byckling and K. Kajantie, *N-particle phase space in terms of invariant momentum transfers*, *Nucl. Phys. B* **9** (1969) 568–576.
- [17] P. D. Draggiotis, A. van Hameren and R. Kleiss, *SARGE: An Algorithm for generating QCD antennas*, *Phys. Lett. B* **483** (2000) 124–130, [hep-ph/0004047].
- [18] A. van Hameren and C. G. Papadopoulos, *A Hierarchical phase space generator for QCD antenna structures*, *Eur. Phys. J. C* **25** (2002) 563–574, [hep-ph/0204055].
- [19] E. Bothmann, T. Childers, W. Giele, F. Herren, S. Hoeche, J. Isaacson et al., *Efficient phase-space generation for hadron collider event simulation*, *SciPost Phys.* **15** (2023) 169, [2302.10449].
- [20] J. Bendavid, *Efficient Monte Carlo Integration Using Boosted Decision Trees and Generative Deep Neural Networks*, 1707.00028.
- [21] M. D. Klimek and M. Perelstein, *Neural Network-Based Approach to Phase Space Integration*, *SciPost Phys.* **9** (2020) 053, [1810.11509].
- [22] I.-K. Chen, M. D. Klimek and M. Perelstein, *Improved neural network Monte Carlo simulation*, *SciPost Phys.* **10** (2021) 023, [2009.07819].
- [23] C. Gao, J. Isaacson and C. Krause, *i-flow: High-dimensional Integration and Sampling with Normalizing Flows*, *Mach. Learn. Sci. Tech.* **1** (2020) 045023, [2001.05486].
- [24] E. Bothmann, T. Janßen, M. Knobbe, T. Schmale and S. Schumann, *Exploring phase space with Neural Importance Sampling*, *SciPost Phys.* **8** (2020) 069, [2001.05478].
- [25] C. Gao, S. Höche, J. Isaacson, C. Krause and H. Schulz, *Event Generation with Normalizing Flows*, *Phys. Rev. D* **101** (2020) 076002, [2001.10028].

- [26] K. Danziger, T. Janßen, S. Schumann and F. Siegert, *Accelerating Monte Carlo event generation – rejection sampling using neural network event-weight estimates*, *SciPost Phys.* **12** (2022) 164, [2109.11964].
- [27] T. Heimgel, R. Winterhalder, A. Butter, J. Isaacson, C. Krause, F. Maltoni et al., *MadNIS - Neural multi-channel importance sampling*, *SciPost Phys.* **15** (2023) 141, [2212.06172].
- [28] T. Janßen, D. Maître, S. Schumann, F. Siegert and H. Truong, *Unweighting multijet event generation using factorisation-aware neural networks*, *SciPost Phys.* **15** (2023) 107, [2301.13562].
- [29] T. Heimgel, N. Huetsch, F. Maltoni, O. Mattelaer, T. Plehn and R. Winterhalder, *The MadNIS Reloaded*, *SciPost Phys.* **17** (2024) 023, [2311.01548].
- [30] N. Deuschmann and N. Götz, *Accelerating HEP simulations with Neural Importance Sampling*, *JHEP* **03** (2024) 083, [2401.09069].
- [31] T. Heimgel, O. Mattelaer, T. Plehn and R. Winterhalder, *Differentiable MadNIS-Lite*, 2408.01486.
- [32] F. A. Berends and W. T. Giele, *Recursive Calculations for Processes with  $n$  Gluons*, *Nucl. Phys. B* **306** (1988) 759–808.
- [33] F. Caravaglios and M. Moretti, *An algorithm to compute Born scattering amplitudes without Feynman graphs*, *Phys. Lett. B* **358** (1995) 332–338, [hep-ph/9507237].
- [34] F. Caravaglios, M. L. Mangano, M. Moretti and R. Pittau, *A New approach to multijet calculations in hadron collisions*, *Nucl. Phys. B* **539** (1999) 215–232, [hep-ph/9807570].
- [35] P. Draggiotis, R. H. P. Kleiss and C. G. Papadopoulos, *On the computation of multigluon amplitudes*, *Phys. Lett. B* **439** (1998) 157–164, [hep-ph/9807207].
- [36] M. L. Mangano, M. Moretti, F. Piccinini, R. Pittau and A. D. Polosa, *ALPGEN, a generator for hard multiparton processes in hadronic collisions*, *JHEP* **07** (2003) 001, [hep-ph/0206293].
- [37] C. Duhr, S. Hoeche and F. Maltoni, *Color-dressed recursive relations for multi-parton amplitudes*, *JHEP* **08** (2006) 062, [hep-ph/0607057].
- [38] O. Mattelaer and K. Ostrolenk, *Speeding up MadGraph5\_aMC@NLO*, *Eur. Phys. J. C* **81** (2021) 435, [2102.00773].
- [39] S. Keppeler and M. Sjödalh, *Orthogonal multiplet bases in  $SU(N_c)$  color space*, *JHEP* **09** (2012) 124, [1207.0609].
- [40] R. Frederix and T. Vitos, *The colour matrix at next-to-leading-colour accuracy for tree-level multi-parton processes*, *JHEP* **12** (2021) 157, [2109.10377].
- [41] S. Badger, B. Biedermann, P. Uwer and V. Yundin, *Numerical evaluation of virtual corrections to multi-jet production in massless QCD*, *Comput. Phys. Commun.* **184** (2013) 1981–1998, [1209.0100].
- [42] R. Britto, F. Cachazo and B. Feng, *New recursion relations for tree amplitudes of gluons*, *Nucl. Phys. B* **715** (2005) 499–522, [hep-th/0412308].

- [43] S. J. Parke and T. R. Taylor, *An Amplitude for  $n$  Gluon Scattering*, *Phys. Rev. Lett.* **56** (1986) 2459.
- [44] L. J. Dixon, J. M. Henn, J. Plefka and T. Schuster, *All tree-level amplitudes in massless QCD*, *JHEP* **01** (2011) 035, [1010.3991].
- [45] J. R. Andersen and J. M. Smillie, *Multiple Jets at the LHC with High Energy Jets*, *JHEP* **06** (2011) 010, [1101.5394].
- [46] D. Zeppenfeld, *Diagonalization of Color Factors*, *Int. J. Mod. Phys. A* **3** (1988) 2175–2179.
- [47] P. Nason, *MINT: A Computer program for adaptive Monte Carlo integration and generation of unweighted distributions*, 0709.2085.
- [48] R. D. Ball et al., *Parton distributions with LHC data*, *Nucl. Phys. B* **867** (2013) 244–289, [1207.1303].
- [49] S. Frixione and B. R. Webber, *Matching NLO QCD computations and parton shower simulations*, *JHEP* **06** (2002) 029, [hep-ph/0204244].
- [50] R. Frederix, S. Frixione, S. Prestel and P. Torrielli, *On the reduction of negative weights in MC@NLO-type matching procedures*, *JHEP* **07** (2020) 238, [2002.12716].
- [51] P. Nason, *A New method for combining NLO QCD with shower Monte Carlo algorithms*, *JHEP* **11** (2004) 040, [hep-ph/0409146].